Oscillatory solitons and time-resolved phase locking of two polariton condensates

Gabriel Christmann[1,2]**, Guilherme Tosi**[1,3,4]**, Natalia G Berloff**[5,6]**,
Panagiotis Tsotsis**[7]**, Peter S Eldridge**[2]**, Zacharias Hatzopoulos**[2,8]**,
Pavlos G Savvidis**[2,7] **and Jeremy J Baumberg**[1]

[1] Nanophotonics Centre, Cavendish Laboratory, University of Cambridge, J J Thomson Ave, Cambridge CB3 0HE, UK
[2] FORTH-IESL, PO Box 1527, 71110 Heraklion, Crete, Greece
[3] Departamento de Física de Materiales, Universidad Autónoma de Madrid, Madrid E-28049, Spain
[4] Centre for Quantum Computation and Commmunication Technology, University of New South Wales, Sydney, NSW 2052, Australia
[5] Department of Applied Mathematics and Theoretical Physics, University of Cambridge, Cambridge CB3 0WA, UK
[6] Skolkovo Institute of Science and Technology Novaya St., 100, Skolkovo 143025, Russian Federation
[7] Department of Materials Science and Technology, University of Crete, PO Box 2208, 71003 Heraklion, Greece
[8] Department of Physics, University of Crete, PO Box 2208, 71003 Heraklion, Greece
E-mail: christmann.gabriel@gmail.com

Abstract

When pumped nonresonantly, semiconductor microcavity polaritons form Bose–Einstein condensates that can be manipulated optically. Using tightly-focused excitation spots, radially expanding condensates can be formed in close proximity. Using high time resolution streak camera measurements we study the time dependent properties of these macroscopic coherent states. By coupling this method with interferometry we observe directly the phase locking of two independent condensates in time, showing the effect of polariton–polariton interactions. We also directly observe fast spontaneous soliton-like oscillations of the polariton cloud trapped between the pump spots, which can be either dark or bright solitons. This transition from dark to bright is a consequence of the

change of sign of the nonlinearity which we propose is due to the shape of the polariton dispersion leading to either positive or negative polariton effective mass.

S Online supplementary data available from stacks.iop.org/njp/16/103039/mmedia

Keywords: microcavity polaritons, Bose–Einstein condensation, solitons

1. Introduction

Microcavity (MC) polaritons are quasiparticles resulting from a superposition of Fabry–Perot cavity photons and quantum well (QW) excitons [1]. They retain the characteristics of their underlying components, namely a bosonic character at low densities, a small effective mass from the photonic part and strong Coulomb repulsion from their excitonic part. These features enable stimulated relaxation of cavity polaritons to form a macroscopic coherent state [2]. This phenomenon, termed polariton lasing, occurs when the polariton's relaxation rate to the ground state becomes faster than its loss, which is mainly dominated by photon escape through the cavity mirrors. Polariton lasing has been observed at cryogenic temperatures in II–VI [3], III–V semiconductors [4] and even at room temperature in III-nitrides [5, 6], organics [7], and in ZnO [8]. Depending on the photon-exciton detuning, the appearance of this macroscopic coherent state can either be determined by thermodynamics, in which case a Bose–Einstein condensate appears due to the fast thermalization of polaritons [9–11], or by kinetics [12, 13]. Recently there have been extensive research efforts to study these polariton condensates. On one hand a whole zoology of topological excitations has been revealed: quantized vortices, either pinned to defects [14], resonantly created [15] or engineered in lattices [16], as well as dark [17] and bright [18] solitons. On the other hand propagation of these coherent states has been studied, in particular under resonant excitation, under which conditions evidence of superfluidity has been observed [19, 20]. Due to repulsive polariton–polariton interactions, spontaneous propagation can also be obtained under nonresonant excitation [21], and is observed either in 2D [22–24] or in 1D geometries [25]. Furthermore real-time optical control of the excitation combined with the blue shift of polaritons allows for directly confining and modulating polariton flows [16, 25–28].

In this context we recently achieved confinement of polaritons in a harmonic trap, using a two-spot excitation profile [27]. The polaritons occupy equally separated energy states which are well fit by the solution of the quantum harmonic oscillator. We also showed interferometrically that these multiple energy states have a stable phase relationship, similar to phase-locked lasing modes, which yields an oscillatory behavior of the system. Simulations using the complex Ginzburg–Landau (cGL) equation showed excitations that resembles dark solitons, which can have either a regular oscillatory behavior or a more chaotic one, depending on the conditions [27].

In this paper we report on the dynamics of propagating polariton condensates which are incoherently excited. Recording the time-resolved emission of these strongly-coupled MCs directly reveals many unusual phenomena, the most striking being spontaneous formation of oscillating wavepackets, similar to dark or bright solitons depending on the excitation conditions. With this technique, we are also able to time resolve the expansion of single polariton condensates and study the phase locking of two initially independent polariton
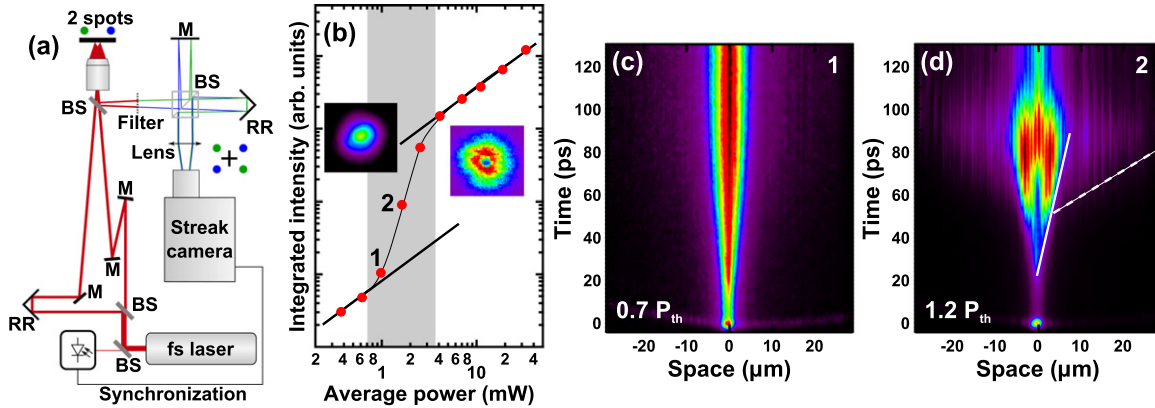
Figure 1. (a) Experiment setup. (b) Time-integrated polariton emission versus pump power, insets are real space emission images. Black lines are guides to the eye above/below threshold at 1.35 mW. (c), (d) Interferometric (see experiment description) time versus space streak camera images, corresponding to 1 and 2 in (b), respectively. White lines in (d) are guides to the eye.

condensates. All these results provide clear and direct observations of the underlying phenomena suggested by continuous wave experiments.

2. Sample description and experiment setup

The MC sample used here consists of a $5\lambda/2$ $Al_{0.3}Ga_{0.7}As$ cavity layer containing four sets of three 10/10 nm $Al_{0.3}Ga_{0.7}As/GaAs$ QWs. It is sandwiched between two $AlAs/Al_{0.15}Ga_{0.85}As$ distributed Bragg reflectors (DBRs), a 32 pair top one and a 35 pair bottom one. The structure exhibits a high quality factor (experimental $Q > 16\,000$) which ensures a long polariton lifetime. Consequently the MC exhibits polariton condensation at low temperature [16, 24, 27, 29]. A detailed study of the nonlinear properties of this sample can be found in [29].

The sample is excited nonresonantly, in the first high energy reflectivity minimum on the edge of the top DBR stopband, at 750 nm using 150 fs pulses from a titanium sapphire laser (repetition rate 76 MHz), unless stated otherwise in the text. We use either one-spot or two-spot excitation profiles, with spot sizes around $1\,\mu m$. In the two-spot case, the delay between the two excitations is kept close to zero. The sample is then directly imaged through a long working distance $\times 100$ microscope objective (numerical aperture 0.7) onto the entrance slit of a Hamamatsu streak camera in synchroscan mode (measured time resolution 2.5 ps). The pump laser is almost completely filtered out and the residual intensity is used as the time origin on our plots. We also exploit motorized translation to perform a full space/time tomography of the emission. To analyse spatial coherence we use a Michelson interferometer with a retroreflector in one arm, which interferes the emission with its symmetric image in a scheme similar to [9]. In the one-spot case the interferometer is aligned so that centre of symmetry is at the excitation spot. In the two-spot case the centre of symmetry is in the middle of the two spots in order to interfere emission from one spot with that from the other. In all the measurements the temperature is kept at ~10 K using a continuous helium flow cryostat. A schematic description of the experimental setup is shown in figure 1(a).

Due to the fact that the streak camera works in synchroscan mode, the measurements are averaged over many experimental realizations. This means that only time-dependent behaviours that are reproducible for every experimental realization will be visible. In the case of spatial coherence measurements, the consequence is that the observation of fringes means that spatially separated areas are locked with the same phase relationship for every experimental realization. Deterministically varying relative phases will appear as a time varying fringe pattern, while stable phase locking will appear as static patterns. On the other hand random phase locking or any slowly varying relative phase will result in a washed out pattern. More detailed discussions in the case of two-spot excitation can be found in the supplementary information. Finally note that the ideal case would be to acquire the emission in single-shot mode, however in our case the emission intensity is too weak. Single-shot measurements of polariton condensate emission have been observed in III-nitride and organic systems known for brighter emission, but even in those case no high time resolution measurements are reported [11, 30].

3. Experimental results

3.1. One-spot measurements

Initially we excite the sample using nonresonantly-tuned pulses which are tightly focused to a single spot of diameter $\sim 1 \mu$m. Power dependent measurements of the time-integrated intensity reveal a clear nonlinear emission threshold associated with polariton lasing (figure 1(b)). The emission is sent through the Michelson interferometer to study spatial coherence, and then to the streak camera whose entrance slit is aligned with the pump spot. The resulting spatio-temporal cuts across the centre of the spot just below and just above threshold are seen in figures 1(c) and (d) respectively. Interferometric measurements show that while no spatial coherence is observed below threshold, above it fringes are clearly observed when interfering areas separated by more than 50μm. The emission pattern is dramatically changed at threshold. While below threshold a slowly increasing emission with slow lateral expansion is observed, above threshold we see a very strong emission appearing after 70 ps which then decays quickly, with a strong lateral expansion (1μm ps^{-1}, white dashed line).

More detailed examination of the polariton expansion in figure 1(d) shows that there are two characteristic expansion speeds (solid and dashed white lines), which we now consider. When the condensate is excited with a tightly focused spot, a local blueshift Δ is created at the pump spot position, where the condensate is created at $k_{\parallel} = 0$ and at the blueshifted energy $E_0 + \Delta$ (where E_0 is the $k_{\parallel} = 0$ polariton energy in the non-blueshifted region) [24]. The condensate then expands radially keeping a constant energy $E_0 + \Delta$ and reaches, far from the excitation spot, a constant in-plane wavevector $k_{\rm c}$ that can be obtained inverting the lower polariton branch dispersion curve. The corresponding polariton ballistic expansion speed is given by the group velocity $\left(v_{\rm g} = \frac{\partial \omega}{\partial k} \right)$. This mechanism is found to correspond to the fast expansion speed (dashed line) as recently also observed in the 1D case [31]. The intense slowly expanding central part occurs in the blueshifted region, where the $k_{\parallel}$ of the condensate is close to zero. This expansion experiences therefore another mechanism rather than simply following the condensate dispersion. We thus believe that this results from the steadily increasing polariton–polariton and polariton–reservoir exciton repulsions in this high polariton density region.
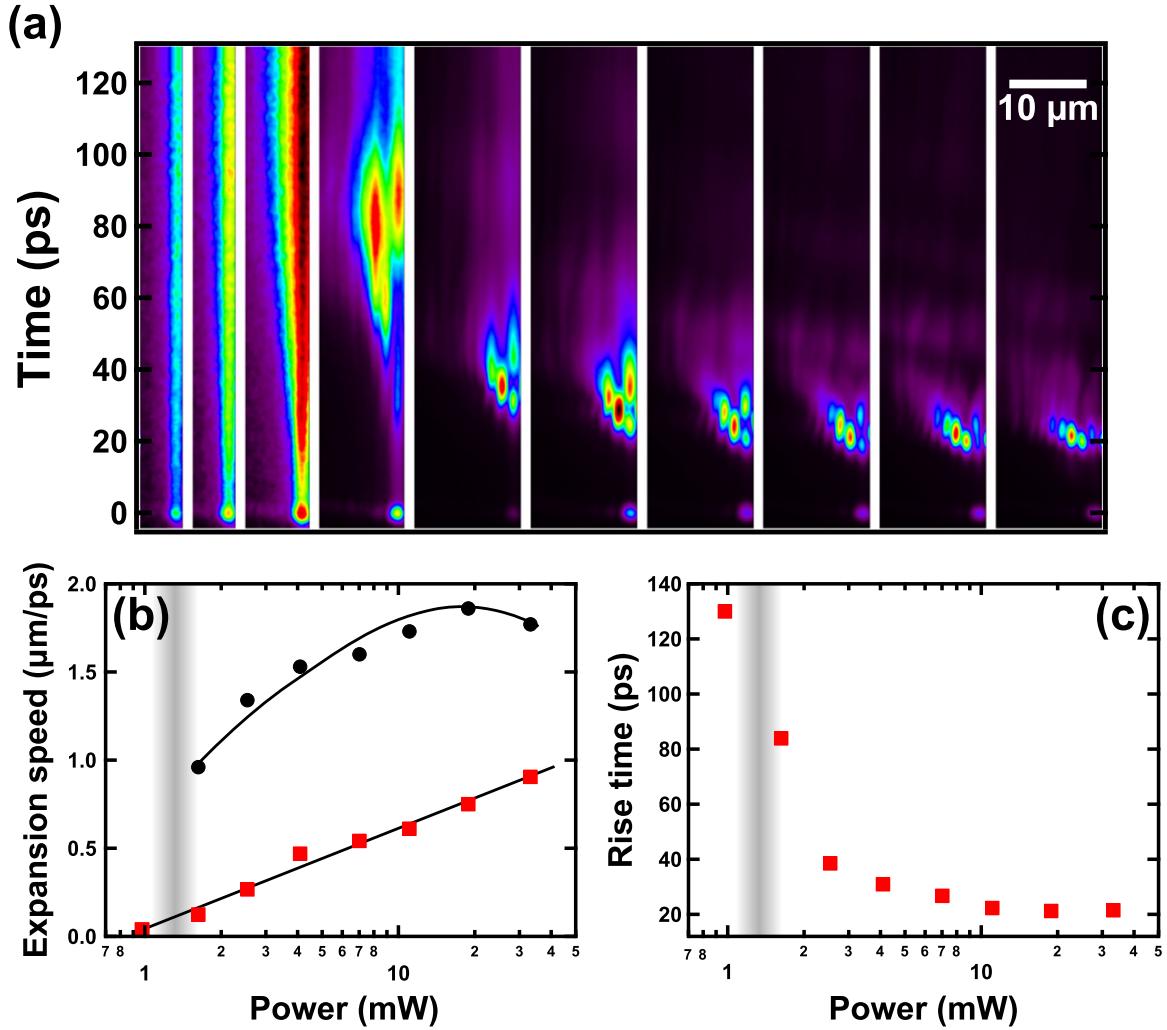
Figure 2. (a) Spatio-temporal dynamics in streak camera images for increasing pump powers ($370\,\mu$W, $620\,\mu$W, $970\,\mu$W, 1.63 mW, 2.54 mW, 4.1 mW, 7.0 mW, 11 mW, 19 mW, 33 mW). (b) Expansion speeds versus pump power corresponding to the slow (solid line in figure 1(d), red squares) and fast (dashed line in figure 1(d), black circles) components. (c) Rise time versus pump power. The grey area in (b) and (c) corresponds to the condensation threshold from figure 1(b).

To gain a deeper understanding of these two expansion speeds, the power dependence of the spatio-temporal emission dynamics is recorded (figure 2(a)) and the extracted speeds reported in figure 2(b). The slower component (red squares) increases steadily with pump power which is a clear signature of the increased repulsive polariton–polariton interactions involved for the dense condensate sat near $k_{\parallel} = 0$. This observation matches the blueshift dependence on power reported previously [24]. We emphasize that this expansion due to repulsive interactions is also visible *below* threshold. Indeed, while no clear expansion is visible for the $370\,\mu$W case, it is increasingly clear in the $620\,\mu$W image and just below the threshold at $970\,\mu$W. On the other hand the fast propagation (black circles) which corresponds to the $k_{\parallel}$ of the condensate in the non-blueshifted area, has a behaviour which departs from that of the slow component. Instead it increases just above threshold and then saturates. This can be understood from the

shape of the lower polariton dispersion curve, and the resulting group velocity ($v_g = \frac{\partial \omega}{\partial k_\parallel}$). In [32] for example, the evolution of v_g versus $k_\parallel$ extracted from the dispersion first increases with $k_\parallel$ until the inflection point in the dispersion curve, and then decreases. This behaviour is indeed very similar to our observations for the fast condensate expansion, with the inflection point passed at a pump power around 20 mW.

The delay to peak emission of the polariton condensate (rise time) versus pump power (figure 2(c)) corresponds to the time at which the spatially-integrated emission reaches its maximum. This rise time decreases quite quickly above threshold, emphasizing the increase of density-dependent polariton–polariton interactions which govern the stimulated scatteing relaxation to the bottom of the trap. It finally reaches a minimum formation time of 20 ps, which probably corresponds to the relaxation of the photocreated electron-hole pairs to hot excitons and then to reservoir excitons.

3.2. Two-spot measurements: mutual coherence

In the continuous wave measurements previously performed on these MCs, two expanding condensates created by separate laser spots exhibited mutual interference fringes [16, 27]. This demonstrated that two separate pumps produce a new single macroscopic coherent state in the steady state regime. This behaviour contrasts with that expected for two independent coherent light sources which are expected to have an unstable phase relation and overlap without showing time-integrated interference. For the nonresonant excitation scheme employed here, the condensate does not retain the coherence properties of the laser [9], so that the locked coherence of the condensate observed is not set by the pump laser. Thus the open question remains how the polaritons created in two separate locations acquire a common phase. Is there an underlying common extended photonic mode that forces the coherence? Do the condensates 'talk' to each other through polariton–polariton interactions to create a common phase? Previous studies have investigated locking phenomena but in disordered potentials without significant polariton propagation. These reported that two (or more) areas of the sample exhibiting different ground state energies below the condensation threshold form a common coherent delocalized single energy state above threshold [33]. Such experiments do not rule out the presence of a common polariton delocalized mode resulting from coupling between two underlying photonic modes. A very similar configuration has been used to create polariton Josephson junctions in MCs [34].

In order to explore these questions we look at the time-resolved emission under two spot pulsed excitation, using tomography. Interferometric images of the two spot emission for various times after excitation (figure 3) show the dynamics of the locking. The emission is sent through the interferometer which interferes with the two spots, with the autocorrelation region being in the centre of the image (figure 1(a)). The tilt between the interferometer mirrors is set to produce oblique interference fringes. The excitation power is chosen slightly above threshold in order to have a reasonably slow expansion speed. Just as the laser spots hit the sample (figure 3(a)) no fringes are observed because the two laser pulses have only just arrived (their arrival time is identical within the 2 ps streak time resolution). The emission from the two condensates shortly after their formation (figure 3(b)) shows limited condensate expansion without any collision yet. While the coherence measurements in figure 1(c) shows that spatial
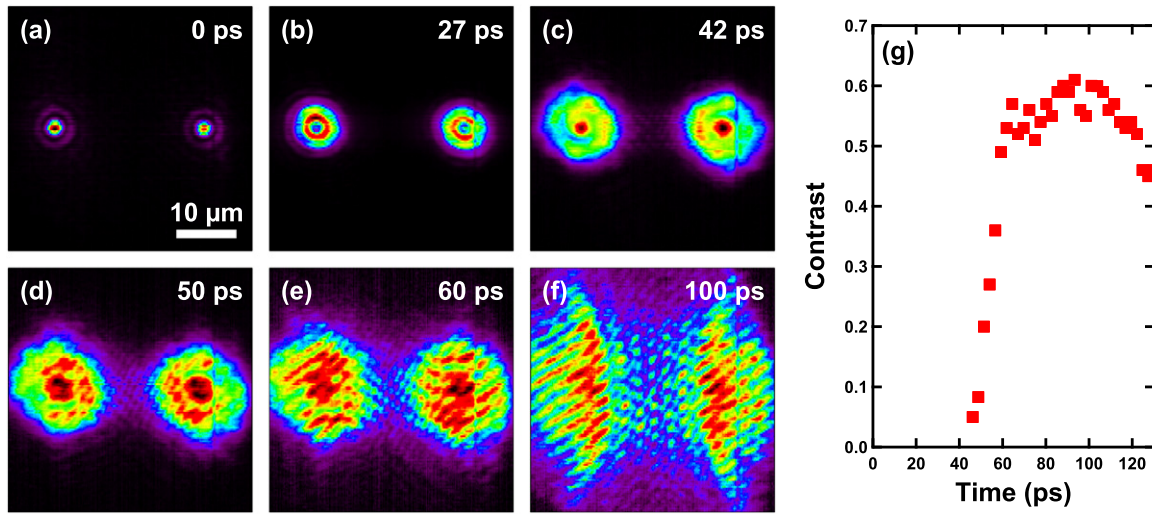
Figure 3. (a)–(f) Interferometric images of the emission at various times illustrating phase locking of two initially independent polariton condensates. (g) Fringe contrast 10–15 μm away from the central autocorrelation spot versus time.

coherence is observed within individual condensates as soon as they form, the absence of fringes in the repeatedly-averaged scans of figure 3(b) show unambiguously that at this time the emissions from each pumped condensate are not phase-locked[7]. Thus in figure 3(b), the two condensates are individually coherent but still independent. After more time (figure 3(c)) the condensates have expanded and come to contact. No fringes are observed in the main condensate emission region, however fringes start to be observed near the central autocorrelation region. At this stage the two condensates are beginning to interact but still have not built up a common phase. After only 8 ps more (figure 3(d)) clear interference fringes are observed within the main condensate emission. This indicates that the two condensates are no longer independent and that a common phase is building up between them, revealing the formation of a new single macroscopic coherent state. We note that the fringe contrast is stronger on the nearest side to the partner spot, revealing that coherence develops from the contact point to the outside. This coherence propagation is faster than the condensate propagation with fringes clearly appearing further away from the individual condensate's expansion. After 18 ps from contact (figure 3(e)) the coherence has extended to the full emission, and finally figure 3(f) shows that after 40 ps more this new macroscopic coherent state has evolved to a steady state pattern similar to those observed under continuous wave excitation [27].

To sum up these observations in a more quantitative way, the dynamical build-up of the fringe contrast ($C = \frac{I_{max} - I_{min}}{I_{max} + I_{min}}$) is reported in figure 3(g). Because the interference fringes are combined with a changing emission pattern, the contrast is measured at the point of maximum emission in a square area of $10 \times 10\,\mu m^2$ located 10–15 μm away from the central region, along the line joining the two spots. The coherence buildup starts to appear at 45 ps and rises to 60% within 20 ps. The contrast then plateaus until 100 ps and then decreases to 45% at 130 ps.

---

[7] If a single shot experiment was possible, drifting fringes would be observed from the two non phase locked coherent light sources with nearly equal energy.

Clearly the time delay of 45 ps before condensate locking is strongly power dependent, because it corresponds to the time at which the expanding condensates come to contact and this expansion speed itself is strongly power dependent (figure 2(b)).

The phase locking is predicted from the coupling in the wavefunction dynamics [28]. To indicate how two condensates will lock together, we explicitly write these cGL equations for interactions between two pumping spots described by ψ_1 and ψ_2 in the Josephson approximation, giving

$$i\partial_t\psi_1 = -\left[\nabla^2 + \left|\psi_1\right|^2 + (1 - u)\left|\psi_2\right|^2 + i\left(\alpha - \sigma\left|\psi_1\right|^2\right) \right]\psi_1 + J\psi_2 \tag{1}$$

and similarly for ψ_2 (written in non-dimensional units) and with $1 - u$ explicitly describing the strength of the repulsive interaction between polaritons generated at different spots. α is the effective gain and σ the gain saturation; J is a symmetry breaking term (see below) [35]. To discuss the dynamics it is convenient to neglect the spatial dynamics and reparametrize using $\psi_{1,2} = \sqrt{\rho_{1,2}}\, \exp^{i(\phi \pm \theta/2)}$, $R = (\rho_1 + \rho_2)/2$, $z = (\rho_1 - \rho_2)/2$, and write coupled equations for θ, R, z (the global phase ϕ does not affect the dynamics). In visualizing the dynamics, one may consider a Bloch vector, defined by $x = \sqrt{(\rho_1\rho_2)}\,\cos\theta$, $y = \sqrt{(\rho_1\rho_2)}\,\sin\theta$, z in terms of the above variables. Since there is pumping and decay, the length of the Bloch vector is not conserved, hence there is a dynamical equation for $R = \sqrt{x^2 + y^2 + z^2}$. The coupled equations have the form

$$\dot{\theta} = -2uz + \frac{2Jz\cos\theta}{\sqrt{R^2 - z^2}}, \tag{2}$$

$$\dot{z} = 2(\alpha - 2\sigma R)z - 2J\sqrt{R^2 - z^2}\,\sin\theta, \tag{3}$$

$$\dot{R} = 2\sigma\left(\frac{\alpha}{\sigma}R - R^2 - z^2 \right). \tag{4}$$

The behaviour of the system can be understood by noticing that the choice of parameters used puts one in the 'Josephson regime' of the Josephson equation, i.e. $uR \gg J$, and that in addition the typical dynamics obey $z \ll R$. In this case, equation (4) simply reduces to $R = \alpha/\sigma$. Then, by eliminating z from equations (2), (3) one finds

$$\ddot{\theta} + 2\alpha\dot{\theta} = 4uJ\alpha/\sigma \sin\theta. \tag{5}$$

This equation describes a damped pendulum, with α, which in our units is proportional to the effective polariton gain, providing the rate of damping provided that two condensates occupy the same region of space. Note that this pendulum differential equation corresponds to a damped harmonic oscillator if $\sin(\theta)$ can be considered linear, and so the equation admits two possible equilibrium solutions:

(i) If $J < 0$, the solution is stable if $\sin(\theta) \approx \theta$ yielding $\theta = 0$,

(ii) If $J > 0$, the solution is stable if $\sin(\theta) \approx -\theta + \pi$ yielding $\theta = \pi$.

These two possible solutions were experimentally observed in [16].

Here the sign of J is determined by the physics of the experiment: the sample disorder, the pumping intensity and the distance between the pumping spots. As the result of these
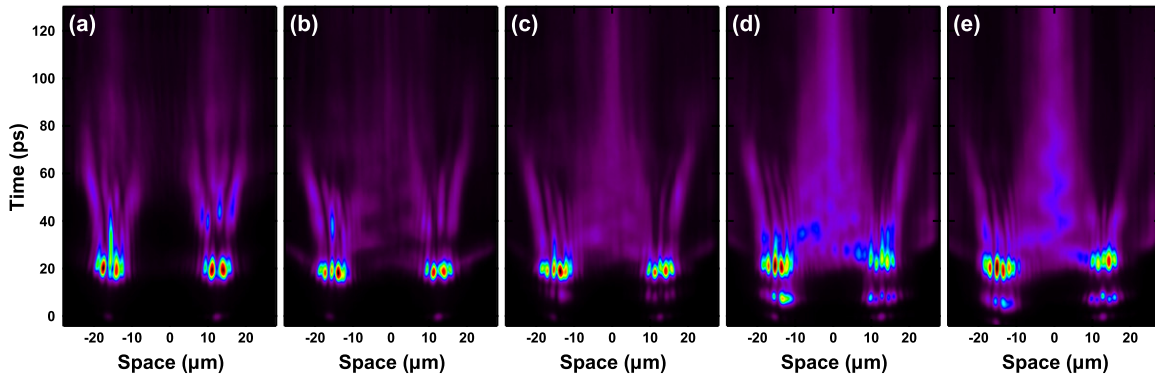
Figure 4. (a)–(e) Spatio-temporal MC emission dynamics under two spot excitation at increasing pump powers (4.5 mW, 11 mW, 16 mW, 24 mW, 28 mW per spot).

experimental conditions the outflowing polaritons of one condensate acquire different phases as they travel across the sample to interact with another condensate, therefore, changing the value of *J*. By changing the distance, the potential landscape (by pumping at different sample locations) or intensity of the pumping spots, we are able to change the sign of *J* and so the lowest energy state of the system: different experimental conditions yield either $\theta = 0$ or $\theta = \pi$ solutions. The similar phase-locking and its dependence on the distance between the pumping spots has been recently reported [36]. The criterion for in-phase and out-of-phase locking was formulated for the system that is trying to minimize the polariton losses and depends on the product of the outflow wave vector at the pumping site and the distance between the spots. Our experiments show that the sample disorder also has an important role (supplementary information, figure S2(a)), so it is a cumulative group velocity acquired by the flow that travels across that sets the locking in our experiments. This is the reason why we can observe interference fringes in between pumping spots even if our time-resolved data are integrated over multiple shot experiments: the specific sample location sets the locking phase in such a way that each individual experimental realization produces the same interference pattern.

In order to experimentally determine the sign of *J* for our time-resolved data, we follow the same procedure as in [16]: the sign of *J* is given by the condensate density in between spots (density minimum means $\theta = \pi$ locking, and therefore $J > 0$, whereas density maximum means $\theta = 0$ locking, and therefore $J < 0$). We clearly see that we have a density minimum between spots, which means antiphase locking (supplementary information, figure S3(e)). Note however that we also find the $J < 0$ situation at different sample locations (supplementary information, figure S2(a)).

This measurement identifies the mechanism of phase locking of polariton condensates. It confirms that the coherence properties from the pump laser are not retained since the two separate condensates created with the same laser are not coherent (until they interact). It shows that the emerging coherence observed in two-spot experiments is due to polariton–polariton interactions as both condensates start to build a coherent phase when they come to contact. This measurement is particularly compelling in the sense that it allows the live observation of the formation of a single macroscopic coherent state from two originally independent ones (see first supplementary video).

3.3. Two-spot measurements: spontaneous oscillations for increasing pump power

When the MC sample is excited by two tightly focused spots, the polariton condensate organizes itself in a harmonic potential and eventually occupies the corresponding quantum harmonic oscillator states, suggesting an oscillatory behaviour that is theoretically expected to resemble to a dark soliton [27]. It is therefore of great interest to investigate the time-dependent emission properties of the sample under such an excitation scheme.

We directly investigate the oscillatory behaviour in time by collecting the emission (without interferometric combination) and align the streak camera slit to the two pump spots (figure 4). With the streak camera operating in synchroscan mode, traces are averaged over many realizations, and therefore an oscillation will be observed only if it appears consistently at every experimental realization. The spatial cuts shown are performed along a line joining the two laser spots. At low powers (figure 4(a)) spatial expansion is observed initially and finally from 60 ps clear fringes are observed in the middle in accordance with the emission patterns observed after long times (vertical fringes between spots in figure 3(f)). This regime corresponds to what is observed under continuous wave excitation at low powers and/or large spot separations. It corresponds to polaritons created at the blushifted energy at the pump spot expanding and phase locking to form the self interference pattern. The polariton density is however too weak to trigger polariton relaxation to the lower states of the harmonic potential and only the top energy state is occupied (supplementary information, figure S2(c)). In this case no oscillatory behaviour is expected.

By raising the power (figure 4(b)), a completely different pattern emerges. A very clear oscillating intensity minimum is observed over more than two full periods in the trap in between the two excitation spots. This observation confirms our previous continuous wave measurements, where we demonstrated that all the polaritons in the different harmonic oscillator levels (supplementary information, figure S3(e)) have a stable phase relationship and therefore should show wavepacket oscillations. Furthermore these measurements confirm the existance of the dark oscillating solitary wave that was predicted by our model [27]. The measured oscillation period is $T = 16$ ps for a $L = 27 \mu$m spot separation. This period is given by $T = \pi L \sqrt{m^*/2\Delta}$ [27], and this measured T is in good agreement with the values measured in the continuous wave case [27].

Surprisingly, when further increasing the pump power, a completely different behaviour is observed (figure 4(c)). The dark soliton oscillation becomes fainter, and by further increasing the injection a bright oscillation starts to appear (figure 4(d)). This becomes increasingly dominant and at the highest power this bright soliton can be observed over three full periods ($T = 15$ ps, similar to the dark case) (figure 4(e)). This transition from dark to bright solitons is very striking as such bright oscillation was not predicted by our previous simulations using the cGL equation. We note that to initially trigger these oscillations we slightly change the time delay of the pump pulses by 3 ps (figure 4(e)) which stabilizes the streak camera images. Streak camera images without optimization can be found in the supplementary information.

From this experimental data it would be interesting to extract the spatial and temporal width of the solitons, as well as their degree of darkness. Unfortunately, streak camera measurements do not allow this, because the temporal resolution of 2.5 ps is not able to resolve the sub-picosecond temporal dynamics (previously measured by time-correlation [27]). The streak data is also acquired through numerous experimental realizations which forms an additional limiting factor. The indicative soliton profiles and extracted soliton darkness/
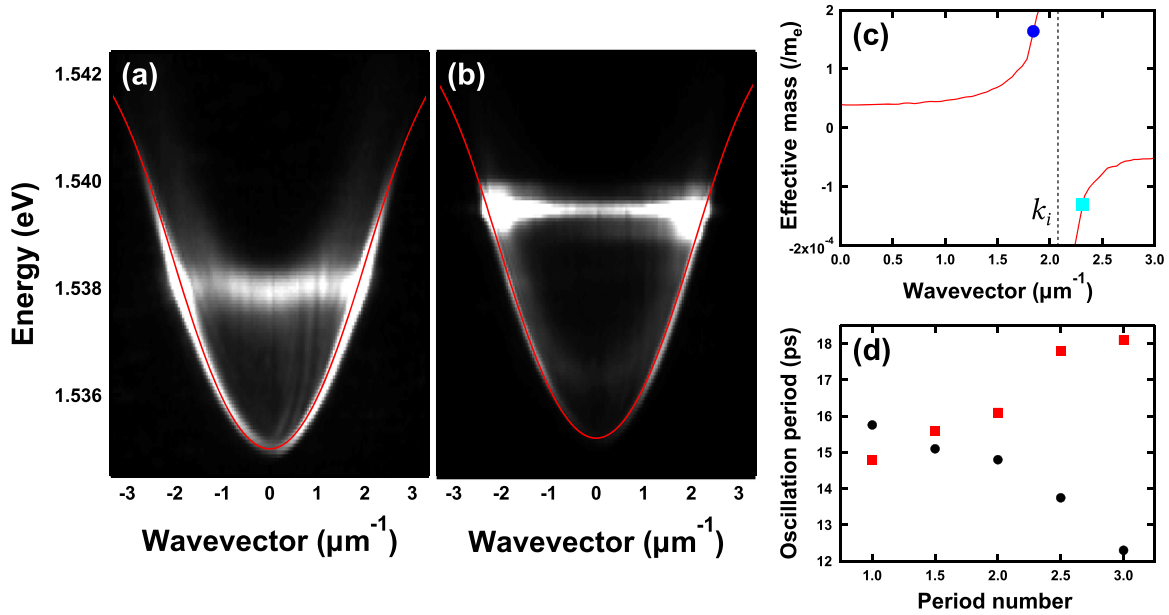
Figure 5. (a)–(b) Image of a *k* space cut versus energy of the polariton emission under single-spot continuous wave pumping for two different powers. Solid red lines are fits of the lower polariton branch. (c) Dispersion of the polariton effective mass deduced from the previous fits. Dark spots correspond to the condensate wavevector in (a), bright spots to the one in (b). (d) Successive individual period duration for the oscillations in figure 4(b) (black circles) and figure 4(e) (red squares).

brightness are reported in supplementary information figure S5, however the measured values should not be taken as an accurate measurement for the reasons mentioned above.

An explanation for this dark to bright transition comes from the the very peculiar shape of the lower polariton dispersion. While one generally adopts a quadratic approximation to the polariton trap, where polaritons have a constant effective mass, the dispersion curve actually has an inflection point at which the effective mass diverges, and at higher wavevectors this mass becomes negative. This point becomes very important for particles with repulsive interactions like polaritons, as dark solitons are expected for positive effective mass, while bright solitons are expected for negative effective mass [17, 18, 37, 38]. As discussed in the one-spot time-resolved measurements, increasing the power leads to larger blueshifts and $k_{\parallel}$, which exceeds the inflection point for pump powers greater than ~ 20 mW. It is therefore possible to have a transition from positive to negative effective mass with increasing blueshift, and thus a transition from dark to bright solitary waves.

To confirm in detail reaching the negative effective mass of polariton condensate at higher pump powers, the experimental dispersion curves from one-spot continuous wave experiments [24] for two pump powers are fit using a 2×2 matrix Hamiltonian describing the coupling between the uncoupled exciton and the cavity mode (figures 5(a) and (b)). In such measurements no spatial selection is performed so emission from blueshifted regions close to the pump spot are collected, as well as non-blueshifted regions outside this, which in fact dominate the images recorded. The contribution from blueshifted regions is seen as the diffuse emission inside the dispersion for smaller $k_{\parallel}$ values. The fit parameters for both figures are the same apart from a small rigid blueshift of $200 \, \mu$eV. The effective mass is obtained from

dispersion curves using $m^* = \hbar^2 \left(\frac{\partial^2 E}{\partial k^2} \right)^{-1}$ and reported in figure 5(c). For the lower power case (dark blue dot) the effective mass is positive whereas it is negative for the higher power case (light blue dot). It is thus indeed possible to change from a positive effective mass condensate to a negative effective mass one only by increasing the pump power, for the case of a single spot. However the situation is more complicated in the two-spot case, and especially when relaxation to lower states is active, as several states are observed in k space (supplementary information, figures S2(d) and (f)), corresponding to the different confined levels in the spatial harmonic potential well (supplementary information, figures S2(c) and (e)). As a result, contrary to the one-spot case, at high excitation power instead of having all polaritons experiencing a negative effective mass, they become anisotropic with part of them experiencing a positive mass and part a negative mass. In spite of this complicated evolution of effective mass, the stable solution for locking between the discrete states may still change from a dark soliton to a bright soliton, as more and more states experience negative effective mass. Numerical simulations are being developed to study this transition from dark to bright, however the full inclusion of the non-parabolicity of the polariton effective mass is challenging. We also discuss in the supplementary information how the cGL equation for a constant effective mass could lead to either focusing or defocusing nonlinearities depending on experimental parameters. In summary, the exact mechanism for the clear switching observed is still under theoretical investigation but the experiment reported here unambiguously shows that the system switches from a regime where the mode locking is stable for dark-solitons, to one where bright-solitons are stable, controlled by excitation power.

Another important point is that these solitons are observed in synchroscan mode, meaning they appear exactly in the same way for every experimental realization. This means that there is a distinct initiation of the soliton in a given reproducible configuration. While the presence of a suitably positioned defect could be an obvious mechanism [17], our observations are performed in a very clean part of the sample. For the sake of comparison, spatio-temporal images in the presence of a defect are reported in figures S4(d)–(f) and produce polariton oscillations similar to those observed in polariton Josephson junctions [34]. Experimentally, tweaking the time delay between the two spots is the only experimental adjustment that has a consistent effect, helping trigger stable streak camera images by breaking the symmetry of the experimental configuration and thus deterministically seeding the solitons. In addition, as mentioned above, adding a small but more significant time delay (<5 ps) helps stabilize the oscillations. This is equivalent to adding some relative phase between the expanding condensates, shifting their resulting interference pattern. A more symmetric configuration (simultaneous pulses) leads to a destructive (dark) interference condition in the middle of the trap (because of the *pi* phase shift when mode locking) and would seed a stable dark soliton, while an asymmetric configuration (with small delay) would shift a constructive condition towards the centre and seed a stable bright soliton. Note that for a fixed pump power, changing the time delay between pulses does not allow us to observe a change between bright and dark oscillations. This is because at a given power the effective mass is either positive or negative, therefore the system can only support one type of oscillation. In summary, the excitation power selects which type of oscillation is stable in the system, and adjusting the time delay allows for more efficient seeding of stable dark or bright oscillations.

A final observation is the contrasting evolution of the oscillation period over time for the bright and dark solitons (figure 5(d)). In the spatio-temporal data we observe that the dark

oscillation period (figure 4(b)) decreases at longer times whereas the bright one (figure 4(e)) increases. As pulsed excitation is employed, the exciton reservoir and polariton density decay with time. This yields a reduction in the confining potential which should always produce a lengthening of the oscillating period [27], clearly not explaining the opposed behaviour for dark-/bright-solitons. Instead the effective mass dispersion better explains this behaviour. As time evolves, the blueshift decreases and the $k_\parallel$ of polaritons away from pump spot decreases as well. From figure 5(c), a decrease of $k_\parallel$ leads to a decrease of effective mass for the dark case whereas it leads to an increase of the magnitude of the effective mass in the bright case. It therefore leads to a contraction of the oscillations in the dark case and a lengthening in the bright case, matching the data well.

Finally, we want to stress that compared to previous reports on solitons [17, 18], our solitary waves spontaneously appear under nonresonant excitation. Additionally, in previous reports the solitons propagated freely through the sample while in our case they are formed only through the mode locking of discrete equally-spaced modes in a harmonic trap [27] leading to dark or bright oscillations depending on the sign of the nonlinearity. In this respect our system has strong connections with soliton lasers (note that mode locking to dark oscillations has been recently reported in semiconductor lasers [39]). Furthermore, it is known that solitons oscillate in the harmonic trap for Bose–Einstein condensates in ultra cold gases, as was predicted theoretically [40–42] and observed experimentally [43]. Another difference arising from the different nature of our soliton formation compared to previous reports is the π phase shift that is observed in the stationary case [17]. As the phase change for dark solitons in the nonlinear Schrödinger equation is proportional to $\arccos(v/c)$, where v is the soliton velocity and c is the speed of sound, the phase varies continuously between 0 and π depending on the degree of soliton darkness [44], so no well defined phase shift is expected in our case.

4. Conclusion

Spatio-temporal dynamical measurements of propagating condensates thus reveal their interactions directly and confirm observations under continuous wave pumping, providing new insights. One-spot measurements allow polariton propagation in the vicinity of and away from the pump spot to be observed separately. We observe the progression of phase locking between two originally independent polariton condensates. This demonstrates that two condensates created with the same laser do not have the same phase initially (as long as they are separated) but thanks to polariton–polariton interactions they build a common condensate immediately that they come into contact. Finally we observe time-resolved soliton oscillations in an optically-imprinted harmonic potential, as suggested by continuous wave measurements. We observe dark oscillations at low power and bright oscillations at high power. In the low power case the stable mode-locked configuration is a dark oscillation due to the positive effective mass and repulsive interactions, while in the high power case the stable dynamics is a bright oscillation arising from sign reversal of the effective mass or from reversal of the defocusing to a focusing nonlinearity.

Acknowledgments

References

[1] Weisbuch C, Nishioka M, Ishikawa A and Arakawa Y 1992 Observation of the coupled exciton-photon mode splitting in a semiconductor quantum microcavity *Phys. Rev. Lett.* **69** 3314–7

[2] Imamoğlu A, Ram R J, Pau S and Yamamoto Y 1996 Nonequilibrium condensates and lasers without inversion: exciton-polariton lasers *Phys. Rev.* A **53** 4250–3

[3] Dang L S, Heger D, Andre R, Bœuf F and Romestain R 1998 Stimulation of polariton photoluminescence in semiconductor microcavity *Phys. Rev. Lett.* **81** 3920–3

[4] Deng H, Weihs G, Santori C, Bloch J and Yamamoto Y 2002 Condensation of semiconductor microcavity exciton polaritons *Science* **298** 199–202

[5] Christopoulos S *et al* 2007 Room-temperature polariton lasing in semiconductor microcavities *Phys. Rev. Lett.* **98** 126405

[6] Christmann G, Butté R, Feltin E, Carlin J-F and Grandjean N 2008 Room temperature polariton lasing in a GaN/AlGaN multiple quantum well microcavity *Appl. Phys. Lett.* **93** 051102

[7] Kéna-Cohen S and Forrest S R 2010 Room-temperature polariton lasing in an organic single-crystal microcavity *Nat. Photonics* **4** 371–5

[8] Guillet T *et al* 2011 Polariton lasing in a hybrid bulk ZnO microcavity *Appl. Phys. Lett.* **99** 161104

[9] Kasprzak J *et al* 2006 Bose–Einstein condensation of exciton polaritons *Nature* **443** 409

[10] Balili R, Hartwell V, Snoke D, Pfeiffer L and West K 2007 Bose–Einstein condensation of microcavity polaritons in a trap *Science* **316** 1007–10

[11] Baumberg J J *et al* 2008 Spontaneous polarization buildup in a room-temperature polariton laser *Phys. Rev. Lett.* **101** 136409

[12] Kasprzak J, Solnyshkov D D, Andre R, Dang L S and Malpuech G 2008 Formation of an exciton polariton condensate: thermodynamic versus kinetic regimes *Phys. Rev. Lett.* **101** 146404

[13] Butté R, Levrat J, Christmann G, Feltin E, Carlin J-F and Grandjean N 2009 Phase diagram of a polariton laser from cryogenic to room temperature *Phys. Rev.* B **80** 233301

[14] Lagoudakis K G, Wouters M, Richard M, Baas A, Carusotto I, André R, Dang L S and Deveaud-Plédran B 2008 Quantized vortices in an exciton-polariton condensate *Nat. Phys.* **4** 706–10

[15] Sanvitto D *et al* 2011 Persistent currents and quantized vortices in a polariton superfluid *Nat. Phys.* **6** 527–33

[16] Tosi G, Christmann G, Berloff N G, Tsotsis P, Gao T, Hatzopoulos Z, Savvidis P G and Baumberg J J 2012 Geometrically-locked vortex lattices in semiconductor quantum fluids *Nat. Commun.* **3** 1243

[17] Amo A *et al* 2011 Polariton superfluids reveal quantum hydrodynamic solitons *Science* **332** 1167–70

[18] Sich M, Krizhanovskii D N, Skolnick M S, Gorbach A V, Hartley R, Skryabin D V, Cerda-Méndez E A, Biermann K, Hey R and Santos P V 2012 Observation of bright polariton solitons in a semiconductor microcavity *Nat. Photonics* **6** 50–5

[19] Amo A *et al* 2009 Collective fluid dynamics of a polariton condensate in a semiconductor microcavity *Nature* **457** 291–5

[20] Amo A, Lefrère J, Pigeon S, Adrados C, Ciuti C, Carusotto I, Houdré R, Giacobino E and Bramati A 2009 Superfluidity of polaritons in semiconductor microcavities *Nat. Phys.* **5** 805–10

[21] Wouters M, Carusotto I and Ciuti C 2008 Spatial and spectral shape of inhomogeneous nonequilibrium exciton-polariton condensates *Phys. Rev.* B **77** 115340

[22] Richard M, Kasprzak J, Romestain R, André R and Dang L S 2005 Spontaneous coherent phase transition of polaritons in CdTe microcavities *Phys. Rev. Lett.* **94** 187401

[23] Wertz E, Ferrier L, Solnyshkov D D, Senellart P, Bajoni D, Miard A, Lemaître A, Malpuech G and Bloch J 2009 Spontaneous formation of a polariton condensate in a planar GaAs microcavity *Appl. Phys. Lett.* **95** 051108

[24] Christmann G, Tosi G, Berloff N G, Tsotsis P, Eldridge P S, Hatzopoulos Z, Savvidis P G and Baumberg J J 2012 Polariton ring condensates and sunflower ripples in an expanding quantum liquid *Phys. Rev.* B **85** 235303

[25] Wertz E *et al* 2010 Spontaneous formation and optical manipulation of extended polariton condensates *Nat. Phys.* **6** 860–4

[26] Amo A, Pigeon S, Adrados C, Houdré R, Giacobino E, Ciuti C and Bramati A 2010 Light engineering of the polariton landscape in semiconductor microcavities *Phys. Rev.* B **82** 081301(R)

[27] Tosi G, Christmann G, Berloff N G, Tsotsis P, Gao T, Hatzopoulos Z, Savvidis P G and Baumberg J J 2012 Sculpting oscillators with light within a nonlinear quantum fluid *Nat. Phys.* **8** 190–4

[28] Cristofolini P, Dreismann A, Christmann G, Franchetti G, Berloff N G, Tsotsis P, Hatzopoulos Z, Savvidis P G and Baumberg J J 2013 Optical superfluid phase transitions and trapping of polariton condensates *Phys. Rev. Lett.* **110** 186403

[29] Tsotsis P, Eldridge P S, Gao T, Tsintzos S I, Hatzopoulos Z and Savvidis P G 2012 Lasing threshold doubling at the crossover from strong to weak coupling regime in GaAs microcavity *New J. Phys.* **14** 023060

[30] Plumhof J D, Stöferle T, Mai L, Scherf U and Mahrt R F 2013 Room-temperature Bose–Einstein condensation of cavity exciton-polaritons in a polymer *Nat. Mater.* **13** 247

[31] Wertz E *et al* 2012 Propagation and amplification dynamics of 1D polariton condensates *Phys. Rev. Lett.* **109** 216404

[32] Szymańska M H, Marchetti F M and Sanvitto D 2010 Propagating wave packets and quantized currents in coherently driven polariton superfluids *Phys. Rev. Lett.* **105** 236402

[33] Baas A, Lagoudakis K G, Richard M, André R, Dang L S and Deveaud-Plédran B 2008 Synchronized and desynchronized phases of exciton-polariton condensates in the presence of disorder *Phys. Rev. Lett.* **100** 170401

[34] Lagoudakis K G, Pietka B, Wouters M, André R and Deveaud-Plédran B 2010 Coherent oscillations in an exciton-polariton Josephson junction *Phys. Rev. Lett.* **105** 120403

[35] Borgh M O, Keeling J and Berloff N G 2010 Spatial pattern formation and polarization dynamics of a nonequilibrium spinor polariton condensate *Phys. Rev.* B **81** 235302

[36] Ohadi H, Gregory R L, Freegarde T, Rubo Y G, Kavokin A V and Lagoudakis P G 2014 Dissipative phase locking of exciton-polariton condensates (arXiv:1406.6377)

[37] Yulin A V, Egorov O A, Lederer F and Skryabin D V 2008 Dark polariton solitons in semiconductor microcavities *Phys. Rev.* A **78** 061801

[38] Egorov O A, Skryabin D V, Yulin A V and Lederer F 2009 Bright cavity polariton solitons *Phys. Rev. Lett.* **102** 153904

[39] Feng M, Silverman K L, Mirin R P and Cundiff S T 2010 Dark pulse quantum dot diode laser *Opt. Express* **18** 13385

[40] Busch T and Anglin J R 2000 Motion of dark solitons in trapped Bose–Einstein condensates *Phys. Rev. Lett.* **84** 2298

[41] Muryshev A, Shlyapnikov G V, Ertmer W, Sengstock K and Lewenstein M 2002 Dynamics of dark solitons in elongated Bose–Einstein condensates *Phys. Rev. Lett.* **89** 110401

[42] Brazhnyi V A and Konotop V V 2003 Evolution of a dark soliton in a parabolic potential: application to Bose–Einstein condensates *Phys. Rev.* A **68** 043613

[43] Weller A, Ronzheimer J P, Gross C, Esteve J, Oberthaler M K, Frantzeskakis D J, Theocharis G and
     Kevrekidis P G 2008 Experimental observation of oscillating and interacting matter wave dark solitons
     Phys. Rev. Lett. **101** 130401
[44] Pitaevskii L P and Stringari S 2003 *Bose–Einstein Condensation* (Oxford: Clarendon) section 5.5